Integrating electrowetting into micromanipulation of liquid droplets

2008 J. Phys.: Condens. Matter 20 485009

(http://iopscience.iop.org/0953-8984/20/48/485009)

J. Phys.: Condens. Matter **20** (2008) 485009 (10pp) doi:10.1088/0953-8984/20/48/485009

Integrating electrowetting into micromanipulation of liquid droplets

Bharat Bhushan[1] **and Xing Ling**

Nanoprobe Laboratory for Bio- and Nanotechnology and Biomimetics (NLB^2), The Ohio State University, 201 W. 19th Avenue, Columbus, OH 43210-1142, USA

E-mail: Bhushan.2@osu.edu

Received 20 August 2008, in final form 16 October 2008
Published 6 November 2008
Online at stacks.iop.org/JPhysCM/20/485009

Abstract
Electrowetting is proposed as a new principle for micromanipulation of a liquid droplet. A conical gripper was used to pick up a droplet and release it onto a substrate by controlling the wetting property between the droplet and the substrate using electrowetting. The rupture process of the liquid bridge between the gripper and the substrate as formed during the pick-up and release stages is studied using a precise numerical method and the arc approximation. The efficiency of micromanipulation is quantified using a term volumetric distribution ratio, which is the volume of the droplet retained by the substrate divided by the whole volume of the liquid droplet during a rupture process, for different combinations of contact angles between the liquid and the gripper or the substrate and the aperture of the conical gripper. Based on the theoretical analysis, an optimized micromanipulation process is suggested which could achieve 100% efficiency by carefully choosing the parameters mentioned above. Preliminary experiments are performed with a commercially available AFM probe to demonstrate this concept. The experimental results are compared with the theoretical prediction proposed here.

(Some figures in this article are in colour only in the electronic version)

1. Introduction

In microscale, surface forces between microcomponents become dominant as compared to the gravitational force of microcomponents. The surface forces are explored and controlled for manipulating microcomponents (i.e. picking up, transporting and releasing) (Frazier and Ahn 1998, Nof 1999, Cecil *et al* 2005). One of the surface forces, capillary force, has recently attracted broad attention as a new principle for micromanipulation (Obata *et al* 2004, Lambert and Delchambre 2005a, Saito *et al* 2005, Lambert *et al* 2006). It is conceived as a non-destructive method as compared to other methods using mechanical or electrostatic forces which might damage the manipulated object due to high stress or discharge current (Obata *et al* 2004). For a typical manipulation cycle based on capillary force, a microsized tool or gripper with a known volume of tiny droplet attached to its head is used to pick up the object from its original location, transport and then release it to the desired location. During the pick-up stage, the capillary force as generated during the formation of the liquid bridge between the gripper and the object needs to overcome the adhesive force between the object and the substrate on which the object sits. For optimal control of the capillary force (i.e. the gripping force), the effects of the droplet volume and the gripper shape have been studied (Obata *et al* 2004, Saito *et al* 2005). However, a large gripping force, as favored during the pick-up stage, might cause a problem during the release stage, where the picked-up object needs to be removed from the gripper. Various strategies of releasing were proposed, namely aids from a droplet sitting on the destination location or an auxiliary sharpened tool, the use of vibrational energy, the rolling of the gripper and the evaporation of the liquid bridge (Obata *et al* 2004, Lambert and Delchambre 2005a, Saito *et al* 2005). Although under limited circumstances these strategies may be successfully applied, none of them is general or versatile enough. New strategies are desired for the continuous development of the capillary method.

One possibility lies in the exploitation of the electrowetting phenomenon. It is known that the wetting property of a conducting liquid on a solid electrode with a dielectric layer between them can be tuned by a potential difference applied to the liquid and the electrode (Quilliet and Berge 2001, Mugele

[1] Author to whom any correspondence should be addressed.

and Baret 2005). The introduction of electrostatic energy reduced the interface tension between the liquid and the substrate, leading to a reduction of the contact angle and enhancing the wetting ability of the liquid (Mugele and Baret 2005). The static and dynamic electrowetting behaviors were intensively studied on conventional and exotic surfaces, for example a nanostructured surface exhibiting superhydrophobicity (Krupenkin *et al* 2004, 2005, 2007). Since the wetting property of the liquid can be locally controlled with high precision using a concentrated electrical field, the integrated patterned electrode has gained popularity during recent years for applications such as transporting, splitting, and merging droplets on a planar surface, which are essential for microfluidic operations (Pollack *et al* 2000, Quilliet and Berge 2001, Cho *et al* 2003, Mugele and Baret 2005). Reversible wetting and de-wetting is another important concern (Sondaghuethorst and Fokkink 1994, Verheijen and Prins 1999, Peykov *et al* 2000, Rosslee and Abbott 2000, Seyrat and Hayes 2001, Mach *et al* 2002, Krupenkin *et al* 2004, 2005, 2007, Dhindsa *et al* 2006, McHale *et al* 2007, Verplanck *et al* 2007, Campbell *et al* 2008). Due to wetting hysteresis, once the droplet spreads on a substrate under the effect of voltage, it tends to remain in the wetting configuration even when the voltage is withdrawn. This renders further manipulation of the droplet using electrowetting difficult. To restore the original configuration of the droplet on a superhydrophobic nanostructured substrate, thermal energy has been inputted by applying a higher voltage than usual to penetrate the insulator to generate a current or heat at the interface between the droplet and substrate to gasify a layer of liquid to detach the droplet from the substrate (Krupenkin *et al* 2004, 2005, 2007). With the introduction of a manipulation system, this problem is intrinsically avoided with an input of mechanical energy to manipulate the droplet. With reversible control of the wetting property of the droplet and consequently the force between the droplet and the substrate in hand, the picking up and releasing can be conveniently realized using electrowetting.

In this paper, the principle of using electrowetting for micromanipulation will be examined. By systematically studying the capillary bridge formed between the gripper and the substrate for different combinations of wetting angles, the effectiveness of manipulation is quantified using a term volumetric distribution ratio, which is the volume retained by the substrate divided by the volume of the liquid bridge during a process that the gripper first contacted and then separated from the substrate with a liquid droplet of known volume bridging them. The liquid transfer between two bodies is a subject for extensive studies especially important for the processing of granular matter (Pepin *et al* 2000, Rossetti *et al* 2003, Lu *et al* 2008, Shi and McCarthy 2008). Here it is of importance as during the pick-up process, the whole droplet would be transferred to the gripper, and during the release stage the whole droplet would detach from the gripper and re-adhere to the substrate. The completely opposite process can happen solely because the wetting property between the liquid droplet and the substrate is modulated, although under certain circumstances the interface between the droplet and gripper can also be conveniently controlled with purposeful design. In addition to the wetting property, the effect of the shape of the gripper will also be studied, which is always an important factor for the manipulation process (Saito *et al* 2005). Also preliminary experiments were carried out using an atomic force microscope (AFM) probe as a microgripper. The results are compared with the principles elucidated here.

2. Experimental details

Electrowetting was performed at both microscale and macroscale. The microscale experiment was performed with a commercial AFM (Dimension 3000, Veeco). A special setup built inside an optical microscope (Optiphot-2, Nikon) was used for the macroscale experiment by moving a thin copper wire using a three-dimensional moving stage. The voltage is drawn from a DC power supply (E3612A, HP). The hydrophobic substrate is prepared by depositing a thin layer of octadecyltrichlorosilane (95%, Acros Organics) (1 mM, toluene solution) onto a silicon oxide surface. The 300 nm thick silicon oxide substrate thermally grown on a p-type boron doped conductive silicon wafer (1–20 Ω cm) was bought from Silicon Quest International. The droplet is taken from a mixture of water, glycerol and salt (1 M) using a 10 μl syringe. The salt is added to render the droplet conductive while the glycerol is added to stabilize the droplet under an open ambient environment. To deposit small droplets (diameter < 100 μm) onto the substrate, a small amount of water mixed with large amount of air is drawn into the syringe, and the syringe is placed close to the substrate and pushed rapidly to release an aerosol containing small droplets to the substrate.

The manipulation process is emulated by first positioning the tip of an AFM probe (VL300, Veeco, nominal spring constant 40 N m^{-1}, front angle 15°, tip height 15–20 μm) onto a droplet (figure 1). After contact is established between the AFM tip and the droplet, the AFM probe is retracted and separated from the droplet. The profiles of the original and residual droplet (if any) are collected *in situ* with the built-in vision system of the AFM. The probe is taken out and examined under the Optiphot-2 optical microscope. Some probes were treated with Piranha solution (H_2O_2:H_2SO_4 = 3:7) at room temperature for 3 h. The treatment greatly reduced their contact angle with water to nearly zero. Such treated probes are also employed for micromanipulation to compare with the untreated probes. The temperature and relative humidity were 21 ± 1 °C and 30 ± 5%, respectively.

3. Results and discussion

A close resemblance to the tilted pyramidal AFM tip would be a cone. A flat surface can be viewed as a cone with an aperture of 180°. Such a connection enables the downsizing of the problem to a liquid bridge confined between two flat surfaces, which we shall examine first. After this, the resemblance and differences between a cone–flat and a flat–flat configuration will be discussed. Based on the above results, the principle of using electrowetting for the manipulation of a liquid droplet will be presented. The experimental results as obtained from different probes will be compared with the principles.

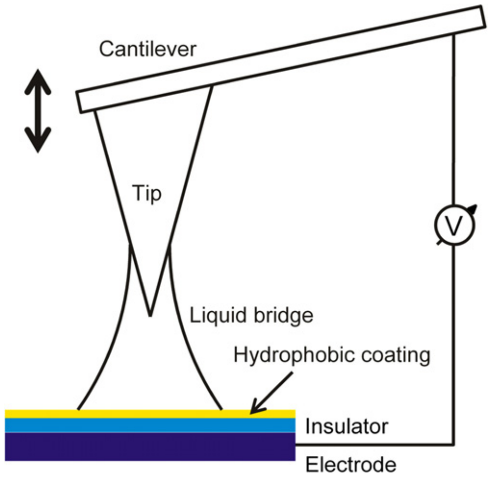

Figure 1. Schematic drawing of the experimental setup used to demonstrate electrowetting-modulated micromanipulation of a liquid droplet. The double arrow indicates the moving direction of the AFM probe.

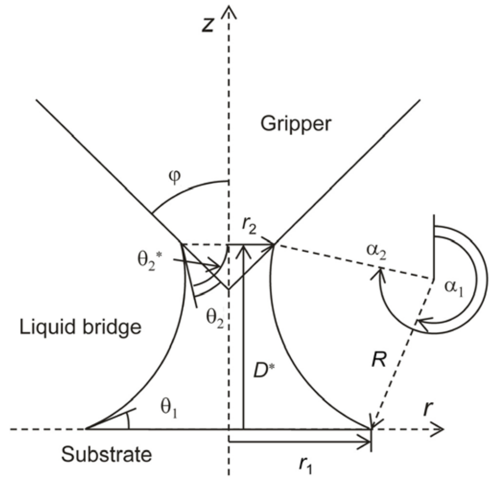

Figure 2. Schematic drawing of the configuration of the liquid bridge confined between a conical gripper and a flat substrate.

3.1. Theory

A liquid of known volume on the order of 1 nl, confined between two solids, is expected to have a uniform mean curvature since the gravitational force is negligible. If it is axially symmetric as shown in figure 2, its mean curvature $\bar{\kappa}$ can be described by Orr *et al* (1975), Lambert and Delchambre (2005b)

$$2\bar{\kappa} = -\frac{r''}{(1+r'^2)^{3/2}} + \frac{1}{r(1+r'^2)^{1/2}} \tag{1}$$

where $r = r(z)$ defines the shape of the liquid bridge with the following boundary conditions: $r_1' = \tan(-\pi/2+\theta_1)$ and $r_2' = \tan(-\pi/2 - \theta_2^*)$. θ_1 is the contact angle between the droplet and the substrate and $\theta_2^* = \theta_2 + \pi/2 - \varphi$ and θ_2 are the effective and true contact angles between the droplet and the gripper.

The equation can only be solved numerically either indirectly by solving an elliptic integral or directly by the trial and error method (Orr *et al* 1975, Fortes 1982, Lambert and Delchambre 2005b). Both require a certain kind of iteration setup, which is difficult as normally multiple solutions exist representing different energy levels. This situation is even worse when the rupture of the liquid bridge and distribution of liquid between two bodies are major concerns. This is the case in the present work, since singularity exists when the neck radius of the liquid bridge approaches zero and jumps among different solutions are likely to occur, which creates difficulties for iteration methods. To circumvent this problem, various researchers have resorted to the arc approximation method (Tselishchev and Val'tsifer 2003, Farshchi-Tabrizi *et al* 2006, Cai and Bhushan 2008). In this way, the axially symmetrical profile of a liquid bridge is approximated by an arc, which takes a position and diameter according to the same boundary conditions as equation (1). While the meridian curvature is fixed, the mean curvature is changing, which is contradictory to equation (1). The physically meaningless approximation however may find great convenience in the study of the rupture of a liquid bridge since it can avoid the difficulty involved in the calculation using equation (1).

Herein, equation (1) is to be solved by a precise numerical method. The numerical method is modified to avoid the common difficulties experienced during the iteration process. It relies on a preformed map of all possible droplet configurations and an interpolating process to locate the exact configuration in the map that best matches the preset conditions. To generate the map, an arbitrary initial location of the contact line between the liquid and the substrate is given. Here we use a value of unity for r_1. With the gradient at $z = 0$ known as $r_1' = \tan(-\pi/2 + \theta_1)$, the droplet profile is uniquely determined by the mean curvature $\bar{\kappa}$. We thus explore the integration results for all possible mean curvatures, theoretically from $-\infty$ to $+\infty$. Here we found that a range from -1 to 1 would be sufficient for most pairs of contact angles we studied. A sufficiently long distance of 10 is used for integration. The integration was actually calculated by using an explicit Runge–Kutta (4, 5) formula, the Dormand–Prince pair, with an error tolerance of 10^{-12}. The integration may stop at a point uniquely under three conditions: (1) $r' = \tan(-\pi/2 - \theta_2^*)$, which means a possible configuration for the droplet, since at this point the effective contact angle of the droplet with the gripper is θ_2^*; (2) r' goes to infinity; and (3) the integration limit of 10 is met. As stopping at condition (1) is set to be of highest priority, stopping at the other two conditions simply means there are no solutions for the specific value of $\bar{\kappa}$. For all valid solutions with integration stopping at condition (1), the volume of droplet encapsulated by rotating the profile obtained during integration around the z axis is calculated using

$$V = \int_{z_1}^{z_2} \pi r^2 \, dz. \tag{2}$$

All parameters, including $\bar{\kappa}$ and the separation distance D, are normalized by this volume. The combination of normalized values of $\bar{\kappa}^*$ and D^* produces a unique one-dimensional space (one curve) for all the possible configurations of droplets for the specified pair of contact angles (θ_1, θ_2^*).

Droplet profiles for representative pairs of contact angles are calculated and plots presented in figure 3(a). Corresponding plots of $\bar{\kappa}^*$ versus D^* are shown in figure 3(b). The results can be classified into three categories, hydrophilic–hydrophilic, hydrophilic–hydrophobic, and hydrophobic–hydrophobic. For the hydrophilic–hydrophilic case, solutions are possible for a mean curvature smaller than a critical value; otherwise, the integration will stop at condition (2). In figure 3(b), it is clear that a maximum separation distance exists for all possible solutions. This distance has been widely recognized as the rupture distance (Lian *et al* 1993). For a separation distance smaller than the maximum, two solutions coexist and the solution with larger curvature is known to be energetically higher than the one with lower curvature and thus unstable. For the hydrophilic–hydrophobic case, the situation is similar except that there are no neck points on the droplet profile ($r' = 0$). For the hydrophobic–hydrophobic case, on the other hand, solutions are only possible for a mean curvature larger than a critical value. Although a maximum distance exists beyond which a solution is impossible, the integration actually stops at condition (3) with undulated droplet profiles exhibiting multiple peaks and valleys. In addition, there is only one solution for a mean curvature higher than the critical value.

The rupture distances as interpolated from figure 3(b) are used for calculating the droplet profile at the moment of rupture. The rupture profiles are plotted in figure 4 for various pairs of contact angles. Also given in figure 4 are profiles obtained using the arc approximation for comparison. The arc profiles are calculated by solving the following equations. The arc is conveniently described using the parameters z_0, r_0, R, and α,

$$z = z_0 + R\cos\alpha \qquad r = r_0 + R\sin\alpha \tag{3}$$

where z_0 and r_0 represent the coordinates of the circular center of the arc, R is the circular radius of the arc, and α is the angle with respect to the z axis clockwise (figure 2). α_1 and α_2 can be directly determined from the contact angles of water and the results are summarized in table 1. At the moment of rupture, only one point on the arc will contact the z axis. Depending on the contact angles, the point would be the top, bottom or middle point of the arc. The results are summarized in table 2. The volume of the liquid bridge as calculated by rotating the arc around the z axis is obtained by combining equations (2) and (3) as

$$V = F(\alpha_2) - F(\alpha_1) \tag{4}$$

where $F(\alpha) = \pi R r_0^2\cos\alpha - \pi R^2 r_0(\alpha - \sin\alpha\cos\alpha) + \frac{\pi R^3}{3}(\sin^2\alpha\cos\alpha + 2\cos\alpha)$. Using the condition given in table 2 and equations (3) and (4), the droplet profile normalized by the volume can be obtained at the moment of rupture of the liquid bridge. The results are plotted in figure 4. They clearly show significant differences from the numerical droplet profiles. The major difference lies in the separation distance at which the liquid bridge ruptures. The arc approximation tends to overestimate the rupture distance, especially for small contact angles.

As for the calculation of volumetric distribution ratio, λ, we found that only when both contact angles are smaller than 90° may splitting of the droplet between the gripper and the substrate happen. Otherwise, the whole droplet will adhere to the body it has a smaller contact angle with. Calculations using numerical methods confirm the same trend. Therefore we focus on the hydrophilic–hydrophilic case for the calculation of λ. Using the arc approximation, the volumetric distribution ratio can be expressed analytically as

Table 1. Determination of the angle α for the arc approximation based on the contact angles.

	α_1	α_2
$\theta_1 + \theta_2^* > \pi$	θ_1	$\pi - \theta_2^*$
$\theta_1 + \theta_2^* < \pi$	$\pi + \theta_1$	$2\pi - \theta_2^*$

Table 2. Determination of the location of the neck point at the rupture distance based on the contact angles.

		Arc contact z axis with	Equivalent condition
$\theta_1 < \pi/2$ and $\theta_2^* < \pi/2$		Middle point	$r_0 = R$
Else	$\theta_1 < \theta_2^*$	Top point	$r_0 = -R\sin\alpha_2$
	$\theta_1 > \theta_2^*$	Bottom point	$r_0 = -R\sin\alpha_1$

$$\lambda = \frac{F(3\pi/2) - F(\alpha_1)}{F(\alpha_2) - F(\alpha_1)} \tag{5}$$

since the neck point has an angle α of 270° with respect to the z axis.

To calculate λ using the numerical method, we need to find the neck point that divides the liquid bridge into two parts. At the neck point $r' = 0$, using interpolation it is straightforward to locate its horizontal coordinates z_n. The volume of liquid encapsulated in the range of $[0, z_n]$ is calculated from equation (2) and then compared with the volume of the liquid bridge to obtain λ. The results are denoted in figure 4. It is surprising that, although the numerical profiles show great discrepancy from the arc profiles, λ are pretty close with an error of 5% for the pair of contact angles of (30°, 60°) we studied. With a difference in contact angles of 30°, about 90% of the droplet goes to the body with the smaller contact angle.

The algorithm derived for the flat–flat configuration can be seamlessly migrated to the cone–flat configuration. The introduction of a conical gripper generally has two effects: (1) the effective contact angle between the liquid and the gripper is increased by an angle of $90° - \varphi$; (2) the tip of the gripper partially immerses in the liquid and occupies space, reducing the volume of liquid the conical gripper can retain. The overall effect of using a conical gripper is to increase the volumetric distribution ratio if other conditions remain the same, which consequently degrades the ability of the gripper to pick up the droplet. However, its ability to release the droplet is enhanced. The calculation is straightforward by taking into account the above two effects. With the effective contact angle $\theta_2^*, \theta_2 + 90° - \varphi$, used, the procedure for calculating the droplet profile is exactly the same. After z_2 is obtained, the volume of the cone is calculated by

$$V_c = \pi z_2^3 \cot\varphi/3 \tag{6}$$

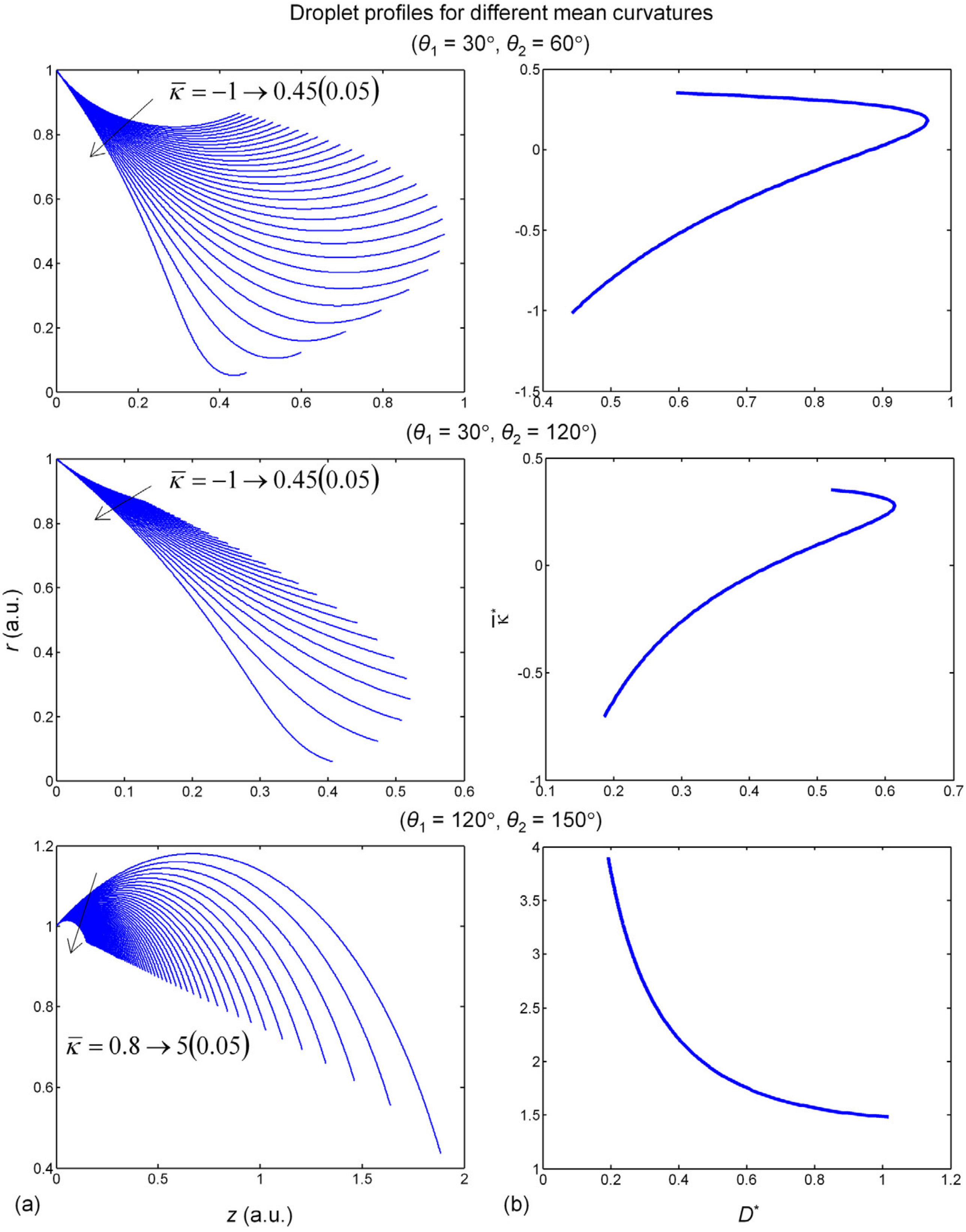

Figure 3. (a) Droplet profiles for a flat–flat configuration derived by numerically integrating equation (1) using different mean curvatures for representative pairs of contact angles (θ_1, θ_2). Volume is calculated from the profiles by solving equation (2). (b) The separation distance and the mean curvature are normalized by the volume and plotted against each other.

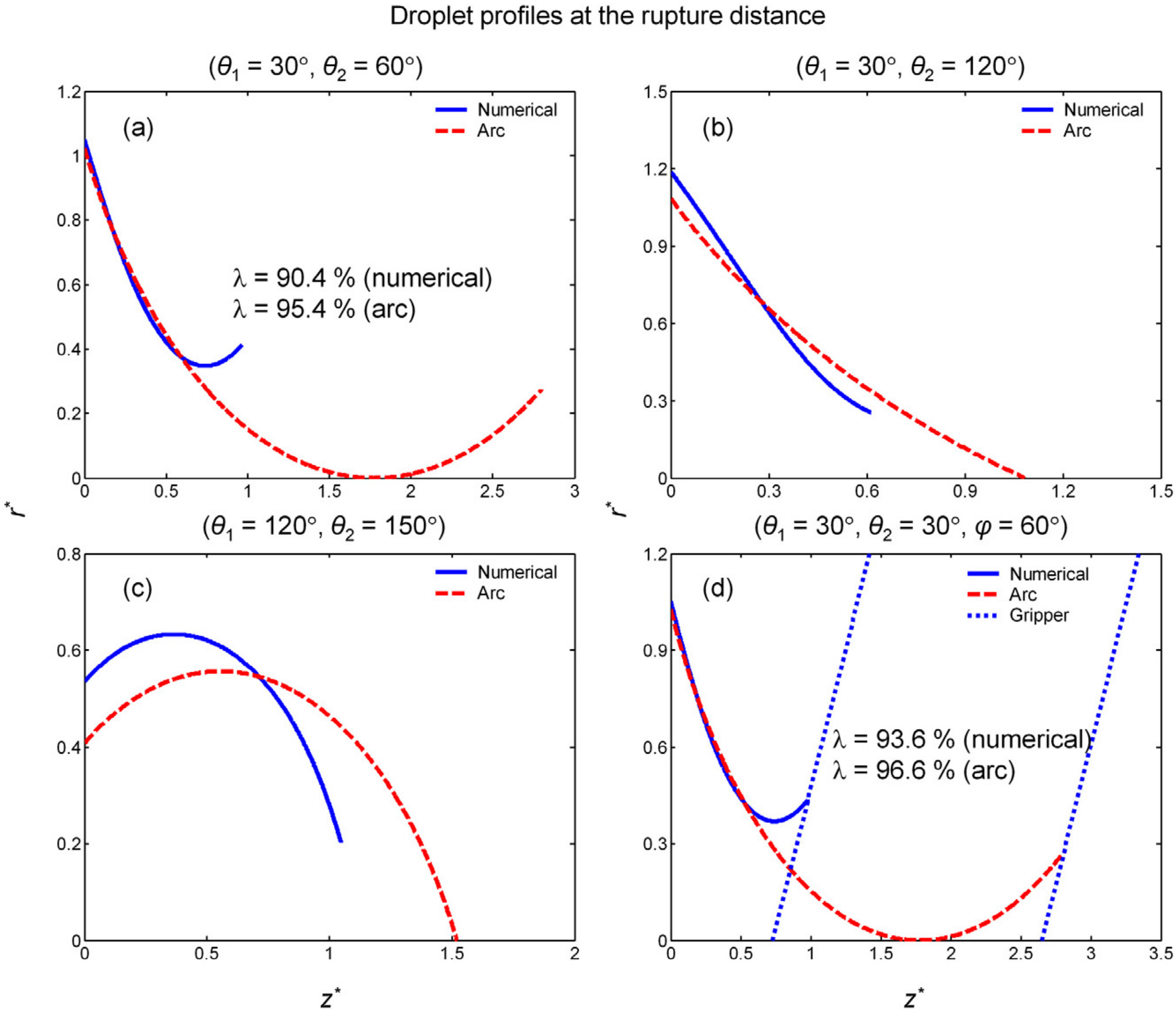

Figure 4. (a)–(c) Droplet profiles for a flat–flat configuration at the rupture distance determined from figure 3(b) for various pairs of contact angles (θ_1, θ_2). (d) Droplet profiles for a cone–flat configuration for a combination of (θ_1, θ_2, φ). Solid lines are results obtained from numerical solution, dashed lines from the arc approximation, and dotted lines in (d) indicate the profiles of the conical gripper. For (a) and (d), volumetric distribution ratios λ are given.

which is subtracted from the volume calculated before using equations (2) or (4). Other parameters are then normalized with this new volume. The criterion for determining the rupture distance is the same. While the effective contact angle remains the same, the effect of conical volume is small. This is verified by comparing the droplet profile in figures 4(d) and (a). The conical gripper in figure 4(d) has a half-aperture of 60° and a reduced contact angle of 30° so that the same effective contact angle of 60° is obtained. The droplet profiles are reasonably close to each other and also the volumetric distribution ratio is only slightly increased by 3%.

One important requirement for using the conical gripper for manipulation is that the liquid wetting angle θ_2 has to be larger than $90° - \varphi$. Otherwise, the droplet may not be able to extend beyond the tip of the cone, and in this case the droplet will retract along the conical gripper and spread behind the tip of the cone. This situation would cause trouble for releasing the droplet since, as the droplet is not able to contact the substrate, it may not be subject to the modulation of the voltage applied between the gripper and the substrate.

3.2. The scheme of manipulation

Based on the above analysis, an efficient scheme of micromanipulation by modulating the wetting property between the droplet and substrate would be as shown in figure 5. For the droplet sitting on the substrate to be effectively picked up by the gripper, the contact angle θ_1 needs to be larger than the effective contact angle θ_2^*. Also, as mentioned above, the selection of a gripper must satisfy the requirement that $\theta_2 > 90° - \varphi$ to allow the picked-up droplet to extend beyond the conical tip. To effectively release the droplet from the gripper, the contact angle θ_1 needs to be reduced to less than the effective contact angle θ_2^*. When θ_1 and θ_2^* are both smaller

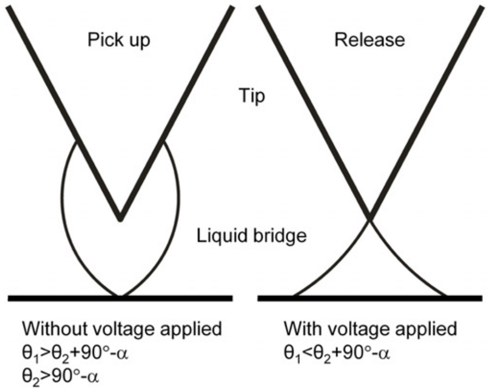

Figure 5. Schematic drawing of an optimized micromanipulation process based on modulating the wetting property between the droplet and the substrate by electrowetting.

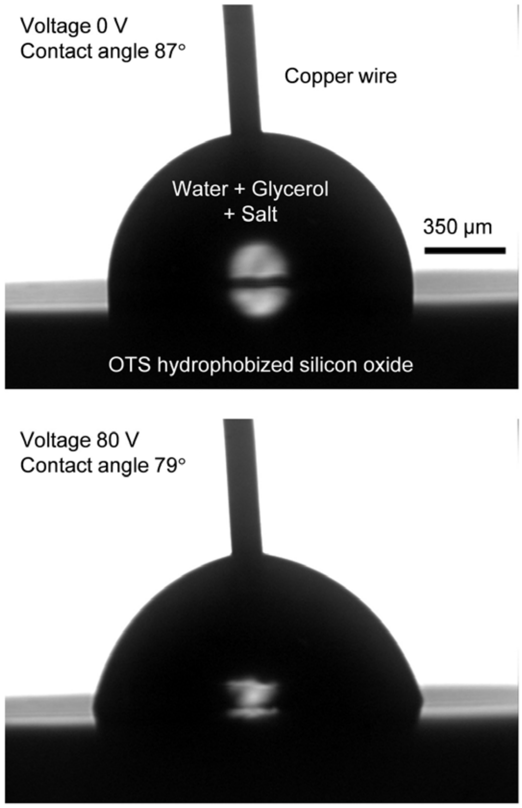

Figure 6. Macroscale electrowetting performed inside an optical microscope using a standard setup.

than 90°, the volumetric distribution ratio would be in the range of (0%, 100%). In principle, to achieve 100% efficiency, θ_2^* has to be larger than 90°. Without the help from the conical gripper, θ_2 would need to be larger than 90°. The requirement can be lowered by half to 45° (as $\theta_2 > 90° - \varphi$) with the introduction of the conical gripper. This is of great advantage as uncleaned metal or ceramic surfaces usually exhibit contact angles close to 45° (in our case, it is about 51°) (Tao and Bhushan 2006). Also, by carefully adjusting the aperture of the cone φ, θ_2^* can be purposely designed to be just slightly above 90°, making the hydrophobization of the substrate much easier as θ_1 only needs to be slightly above 90°, which could be realized using common hydrophobization techniques. In principle, the smaller the difference between the angles θ_1 and θ_2^*, the easier it is to reduce θ_1 below θ_2^* by using electrowetting. However, in reality, due to the wetting hysteresis and the heterogeneity of surface, the difference between them should be large enough to accommodate all these uncertainties. It has been shown by Li and Mugele (2008) that using an AC voltage to replace the DC voltage could reduce the wetting hysteresis to zero if the voltage is large enough, which should be helpful for lowering the voltage requirement to reduce θ_1 below θ_2^*.

3.3. Experimental results

3.3.1. Electrowetting. Here we consider the electrowetting technique used to reduce the contact angle between the droplet and the substrate. The contact angle θ_U depends on the voltage U applied across the droplet and the substrate by the so-called Lippmann equation (Mugele and Baret 2005)

$$\cos\theta_U = \cos\theta_Y + \frac{\varepsilon_0\varepsilon_d}{2d\sigma_{lv}}U^2 \qquad (7)$$

where θ_Y is the Young's contact angle and d and ε_d are the thickness and the dielectric constant of the insulator respectively. ε_0 is the permittivity of vacuum and σ_{lv} is the surface tension of the liquid. For the substrate used in this experiment, we observed a decrease of contact angle from 87° to 79° when a voltage of 80 V was applied (figure 6). However, using equation (7), we would expect the contact angle to be reduced to zero under this voltage for the 300 nm thick insulator. It is likely that contact angle saturation was experienced under this voltage. It is reported that the saturated contact angle increases with the decrease of the thickness of the insulator (Moon *et al* 2002). A saturated contact angle of 80° was found for a 100 nm thick oxide sample, while for a 1 μm thick oxide sample the saturated contact angle slightly decreased to 75° (Moon *et al* 2002). Normally this angle is small enough for θ_1 if the effective contact angle θ_2^* is designed to be larger than 90°. The saturated contact angle can be reduced to as small as ~60° when a 12 μm thick oxide sample is used, which is also a common substrate used in electrowetting experiments (Moon *et al* 2002).

3.3.2. Micromanipulation with an untreated silicon probe. With the measured electrowetting property of the substrate, the micromanipulation behavior of a droplet for different probes will be examined here. The probe we used has a half-aperture of ~15° and a tip height of 15–20 μm. The contribution of the conical tip toward the effective contact angle is 75°, too large for an optimized micromanipulation. Most popular silicon tips commercially available are similarly sharp due to the etching process used to fabricate them. Even for a silicon nitride probe with a much higher half-aperture of about 35° (NP-S, Veeco), the requirement of $\theta_2 > 90° - \varphi$ may not be easily met. Also, the cantilever for a silicon nitride probe is usually too soft to counterbalance the capillary force of 0.1 μN order applied from the droplet. However, we managed to use this silicon tip to achieve a limited success on the electrowetting-

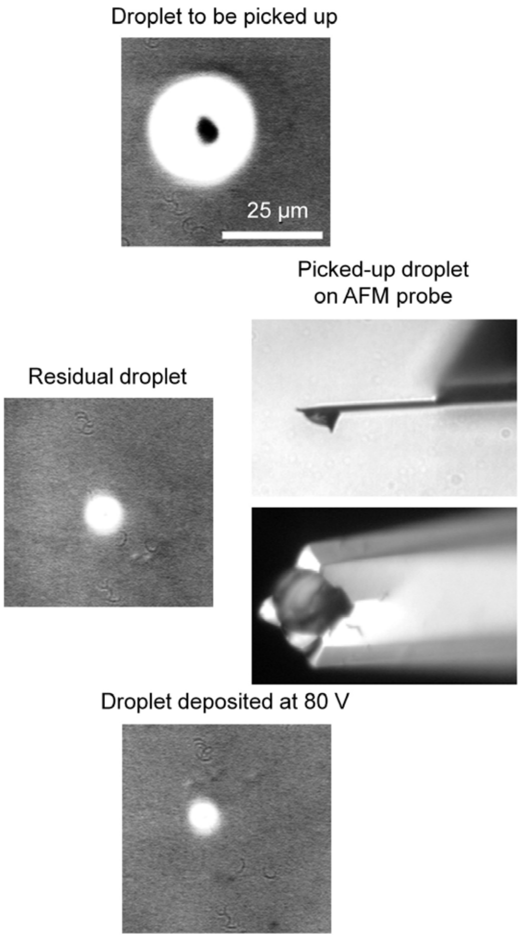

Figure 7. Optical images of the droplets during a micromanipulation process using an untreated AFM probe. The AFM probe is brought into contact and then retracted from the droplet. To redeposit a droplet onto the substrate, a voltage of 80 V is applied after the AFM probe contacted the substrate.

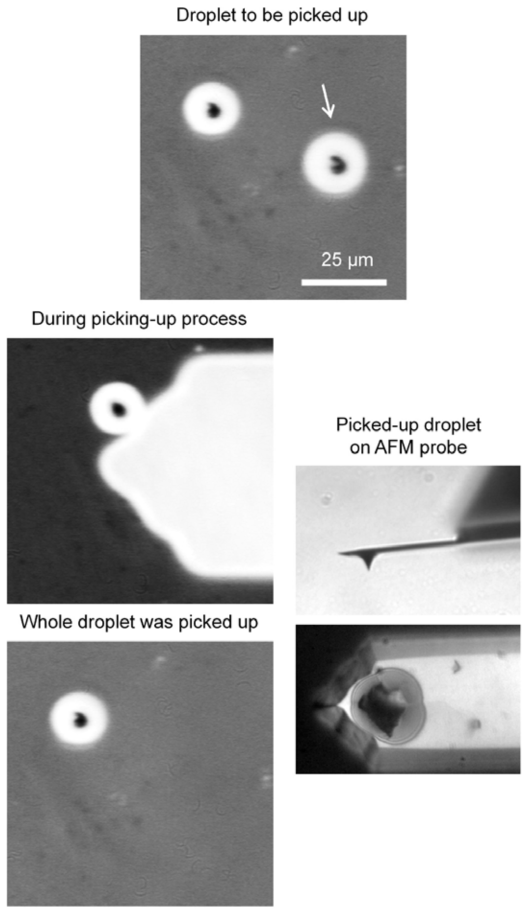

Figure 8. Optical images of the droplets during a micromanipulation process using an untreated AFM probe. The picked-up droplet was unable to be redeposited at a voltage range from 0 to 80 V.

modulated manipulation of the droplet. The result is shown in figure 7. First, the probe is brought into contact with the droplet and then fully retracted from it. An untreated silicon tip could possess a high contact angle of 51° with water (Tao and Bhushan 2006). Thus the effective contact angle θ_2^* would be around 126°, much higher than the contact angle θ_1 of 87°. Therefore, we would expect the silicon tip to be unable to pick up small droplets. Droplets that appear to be higher than the height of the tip may be picked up by the probe. Under this situation, the cantilever supporting the tip may come into contact with the droplet. Its effective contact angle is only 51°, much smaller than the contact angle θ_1 of 87°. After the probe is fully retracted, a tiny droplet is left at the original site, as expected for the splitting of the droplet for a pair of contact angles of (87°, 51°). Since the contact angle θ_2 of 51° is smaller than the $90° - \varphi$ value of 75°, the picked-up droplet is expected to recede away from the tip end, which is observed in the side view image of the probe taken out from the AFM using the Optiphot-2 optical microscope. The receding created difficulty in releasing the droplet. Only under a voltage of 80 V was a tiny droplet able to be deposited from the probe. We hypothesize that as the droplet is relatively large and the difference between the angles θ_2 and $90° - \varphi$ is not too large, even after receding the droplet may be close to the tip end. Under the effect of electrostatic force between the substrate and the probe, the droplet may deform and reestablish contact with the substrate. After this, the reduced contact angle θ_1 requires a redistribution of the droplet between the cantilever and the substrate for the new pair of contact angles of (79°, 51°). This would explain the tiny droplet deposited on the substrate under 80 V as shown in figure 7.

3.3.3. Micromanipulation with a Piranha-treated silicon probe. Micromanipulation was also performed with a Piranha-treated silicon probe. The results are shown in figure 8. The droplet to be manipulated sits at the bottom right with an adjacent droplet serving as a reference. The height of the droplet is much smaller than the one shown in figure 7, preventing the cantilever from contacting with the droplet. After full retraction of the probe, the whole droplet was picked up by the probe as there is no visible residual droplet left at the original site. The water can completely wet the Piranha-treated silicon probe, leaving an effective contact angle θ_2^* of 75°. The volumetric distribution ratio for the pair of contact angles of (87°, 75°) is 0.2% as estimated using the arc approximation. With a little fluctuation on the surface properties of the substrate, it is possible for the probe to completely pick up the droplet. The picked-up droplet receded and almost completely collapsed and spread on the cantilever as expected for the large difference of θ_2 and $90° - \varphi$ of 75°. Since the droplet is far away from the tip end, following attempts to redeposit the droplet back to the substrate were proven to be unsuccessful with a maximum voltage of 80 V tried.

These two experiments, although not performed under optimized conditions, did reveal the important factors for integrating electrowetting into micromanipulation such as the selection of pairs of contact angles and the importance of the shape of gripper. These two factors provide flexibility and versatility for the design of the gripper and substrate by controlling the micromanipulation from different aspects, material properties and geometry.

4. Summary

In this paper, we proposed to use electrowetting to control the wetting property between a microdroplet and a substrate to facilitate a gripper to pick up and release the droplet at will for the purpose of manipulating microdroplets. It is found that by systematically studying the rupture of the capillary bridge formed between a conical gripper and a substrate using both a numerical method and the arc approximation, the volumetric distribution ratio λ, i.e. the volume retained by the substrate divided by the volume of the liquid droplet during a rupture process, strongly depends on the contact angles between the liquid and the gripper or the substrate, θ_2 and θ_1, and the half-aperture φ of the conical gripper. For different combinations of wetting angles and aperture, we found that if either one of the angles θ_1 or the effective contact angle θ_2^*, $\theta_2 + 90° - \varphi$, is larger than 90°, the volumetric distribution ratio could be 0% if $\theta_1 > \theta_2^*$ or 100% if $\theta_1 < \theta_2^*$, while 0% corresponds to an ideal pick-up process and 100% to an ideal release process. If both of the angles are smaller than 90°, the droplet will split between the gripper and the substrate. Under this situation, the volumetric distribution ratio is in the range of 0%–100% and can be solved precisely using the numerical method we suggested or simply using the arc approximation. In addition, for the picked-up droplet to extend beyond the tip end of the gripper, θ_2 has to be larger than $90° - \varphi$, which is important for the releasing of the droplet to the substrate. In summary, for an optimized micromanipulation process, to pick up a droplet from a substrate θ_1 was designed to be initially larger than θ_2^*, and to release the droplet back to the substrate electrowetting was used to reduce θ_1 to be smaller than θ_2^*. If θ_2^* is selected to be larger than 90°, the efficiency could reach 100%, where the whole droplet could be picked up and released at will. Experiments performed with a commercially available AFM probe were used to demonstrate this concept. Although the shape of the tip and the contact angles do not fall in the optimized ranges, the micromanipulation of the droplet was essentially realized in terms of picking up and releasing the droplet using the untreated probe. The micromanipulation process was carefully examined using the principles we proposed here, and the experimental evidence conforms to the theoretical prediction.

References

Cai S and Bhushan B 2008 Meniscus and viscous forces during separation of hydrophilic and hydrophobic surfaces with liquid-mediated contacts *Mater. Sci. Eng.* R **61** 78–106

Campbell J L, Breedon M, Latham K and Kalantar-Zadeh K 2008 Electrowetting of superhydrophobic ZnO nanorods *Langmuir* **24** 5091–8

Cecil J, Vasquez D and Powell D 2005 A review of gripping and manipulation techniques for micro-assembly applications *Int. J. Prod. Res.* **43** 819–28

Cho S K, Moon H J and Kim C J 2003 Creating, transporting, cutting, and merging liquid droplets by electrowetting-based actuation for digital microfluidic circuits *J. Microelectromech. Syst.* **12** 70–80

Dhindsa M S, Smith N R, Heikenfeld J, Rack P D, Fowlkes J D, Doktycz M J, Melechko A V and Simpson M L 2006 Reversible electrowetting of vertically aligned superhydrophobic carbon nanofibers *Langmuir* **22** 9030–4

Farshchi-Tabrizi M, Kappl M, Cheng Y J, Gutmann J and Butt H J 2006 On the adhesion between fine particles and nanocontacts: an atomic force microscope study *Langmuir* **22** 2171–84

Fortes M A 1982 Axisymmetric liquid bridges between parallel plates *J. Colloid Interface Sci.* **88** 338–52

Frazier A B and Ahn C H (ed) 1998 *Proc. SPIE* **3515** 2–291

Krupenkin T, Taylor J A, Kolodner P and Hodes M 2005 Electrically tunable superhydrophobic nanostructured surfaces *Bell Labs Tech. J.* **10** 161–70

Krupenkin T N, Taylor J A, Schneider T M and Yang S 2004 From rolling ball to complete wetting: the dynamic tuning of liquids on nanostructured surfaces *Langmuir* **20** 3824–7

Krupenkin T N, Taylor J A, Wang E N, Kolodner P, Hodes M and Salamon T R 2007 Reversible wetting-dewetting transitions on electrically tunable superhydrophobic nanostructured surfaces *Langmuir* **23** 9128–33

Lambert P and Delchambre A 2005a A study of capillary forces as a gripping principle *Assem. Autom.* **25** 275–83

Lambert P and Delchambre A 2005b Parameters ruling capillary forces at the submillimetric scale *Langmuir* **21** 9537–43

Lambert P, Seigneur F, Koelemeijer S and Jacot J 2006 A case study of surface tension gripping: the watch bearing *J. Micromech. Microeng.* **16** 1267–76

Li F and Mugele F 2008 How to make sticky surfaces slippery: contact angle hysteresis in electrowetting with alternating voltage *Appl. Phys. Lett.* **92** 244108

Lian G P, Thornton C and Adams M J 1993 A theoretical-study of the liquid bridge forces between 2 rigid spherical bodies *J. Colloid Interface Sci.* **161** 138–47

Lu N, Lechman J and Miller K T 2008 Experimental verification of capillary force and water retention between uneven-sized spheres *J. Eng. Mech.-ASCE* **134** 385–95

Mach P, Krupenkin T, Yang S and Rogers J A 2002 Dynamic tuning of optical waveguides with electrowetting pumps and recirculating fluid channels *Appl. Phys. Lett.* **81** 202–4

McHale G, Herbertson D L, Elliott S J, Shirtcliffe N J and Newton M I 2007 Electrowetting of nonwetting liquids and liquid marbles *Langmuir* **23** 918–24

Moon H, Cho S K, Garrell R L and Kim C J 2002 Low voltage electrowetting-on-dielectric *J. Appl. Phys.* **92** 4080–7

Mugele F and Baret J C 2005 Electrowetting: from basics to applications *J. Phys.: Condens. Matter* **17** R705–74

Nof S Y (ed) 1999 *Handbook of Industrial Robotics* 2nd edn (New York: Wiley)

Obata K J, Motokado T, Saito S and Takahashi K 2004 A scheme for micro-manipulation based on capillary force *J. Fluid Mech.* **498** 113–21

Orr F M, Scriven L E and Rivas A P 1975 Pendular rings between solids—meniscus properties and capillary force *J. Fluid Mech.* **67** 723–42

Pepin X, Rossetti D, Iveson S M and Simons S J R 2000 Modeling the evolution and rupture of pendular liquid bridges in the presence of large wetting hysteresis *J. Colloid Interface Sci.* **232** 289–97
Peykov V, Quinn A and Ralston J 2000 Electrowetting: a model for contact-angle saturation *Colloid Polym. Sci.* **278** 789–93
Pollack M G, Fair R B and Shenderov A D 2000 Electrowetting-based actuation of liquid droplets for microfluidic applications *Appl. Phys. Lett.* **77** 1725–6
Quilliet C and Berge B 2001 Electrowetting: a recent outbreak *Curr. Opin. Colloid Interface Sci.* **6** 34–9
Rossetti D, Pepin X and Simons S J R 2003 Rupture energy and wetting behavior of pendular liquid bridges in relation to the spherical agglomeration process *J. Colloid Interface Sci.* **261** 161–9
Rosslee C and Abbott N L 2000 Active control of interfacial properties *Curr. Opin. Colloid Interface Sci.* **5** 81–7
Saito S, Motokado T, Obata K J and Takahashi K 2005 Capillary force with a concave probe-tip for micromanipulation *Appl. Phys. Lett.* **87** 3
Seyrat E and Hayes R A 2001 Amorphous fluoropolymers as insulators for reversible low-voltage electrowetting *J. Appl. Phys.* **90** 1383–6
Shi D L and McCarthy J J 2008 Numerical simulation of liquid transfer between particles *Powder Technol.* **184** 64–75
Sondaghuethorst J A M and Fokkink L G J 1994 Potential-dependent wetting of electroactive ferrocene-terminated alkanethiolate monolayers on gold *Langmuir* **10** 4380–7
Tao Z H and Bhushan B 2006 Wetting properties of AFM probes by means of contact angle measurement *J. Phys. D: Appl. Phys.* **39** 3858–62
Tselishchev Y G and Val'tsifer V A 2003 Influence of the type of contact between particles joined by a liquid bridge on the capillary cohesive forces *Colloid J.* **65** 385–9
Verheijen H J J and Prins M W J 1999 Reversible electrowetting and trapping of charge: model and experiments *Langmuir* **15** 6616–20
Verplanck N, Galopin E, Camart J C, Thomy V, Coffinier Y and Boukherrou R 2007 Reversible electrowetting on superhydrophobic silicon nanowires *Nano Lett.* **7** 813–7